

---

# DEEP GEOMETRIC DISTILLATION NETWORK FOR COMPRESSIVE SENSING MRI\*

---

A PREPRINT

**Xiaohong Fan, Yin Yang, Jianping Zhang<sup>†</sup>**

School of mathematics and computational science

Xiangtan University

Xiangtan, P. R. China

`fanxiaohong@smail.xtu.edu.cn, {yangyinx, jpzhang}@xtu.edu.cn`

May 24, 2022

## ABSTRACT

Compressed sensing (CS) is an efficient method to reconstruct MR image from small sampled data in  $k$ -space and accelerate the acquisition of MRI. In this work, we propose a novel deep geometric distillation network which combines the merits of model-based and deep learning-based CS-MRI methods, it can be theoretically guaranteed to improve geometric texture details of a linear reconstruction. Firstly, we unfold the model-based CS-MRI optimization problem into two sub-problems that consist of image linear approximation and image geometric compensation. Secondly, geometric compensation sub-problem for distilling lost texture details in approximation stage can be expanded by Taylor expansion to design a geometric distillation module fusing features of different geometric characteristic domains. Additionally, we use a learnable version with adaptive initialization of the step-length parameter, which allows model more flexibility that can lead to convergent smoothly. Numerical experiments verify its superiority over other state-of-the-art CS-MRI reconstruction approaches. The source code will be available at <https://github.com/fanxiaohong/Deep-Geometric-Distillation-Network-for-CS-MRI>.

**Keywords** MRI Reconstruction · Compressive Sensing · Deep Geometric Distillation Network · Taylor Expansion

## 1 Introduction

Magnetic Resonance Imaging (MRI) is a widely used medical imaging modality for clinical diagnosis. Nyquist sampling theory has guided the signal sampling process for many years. Strict sampling requirements put a great burden on processing equipment. CS-MRI [8] applies the sparse characteristics of signals in  $k$ -space to image reconstruction, and the sampling rate is much lower than Nyquist sampling rate, but the image quality is not significantly reduced.

Classical CS-MRI methods can be explored in a specific transformation domain or in a generic dictionary-based subspace to learn more flexible sparse representation directly from data [13]. Although Total Variation (TV) regularization in the gradient domain introduces staircase artifacts in reconstructed image, it has been widely used in MRI reconstruction due to simple and fast [5]. Discrete wavelet transform [11] and discrete cosine transform [12] have also been utilized to reconstruct CS-MRI. Many iterative algorithms such as Iterative Shrinkage Threshold Algorithm (ISTA) [2] and Alternating Direction Multiplier (ADMM) [6] have been designed to solve CS-MRI models. These CS-MRI methods are all based on interpretable and predefined sparsity image prior rather than direct learning, but cannot obtain desirable reconstruction results. Although most of these methods have the advantages of theoretical analysis and strong convergence, they usually require expensive computational complexity to converge, and also face the difficulties of selecting the regularizer and model parameter.

---

\* Accepted by IEEE-EMBS International Conference on Biomedical and Health Informatics (BHI), 2021 (Oral).

<sup>†</sup>Corresponding author: `jpzhang@xtu.edu.cn` (J. Zhang).

Recently, deep learning has received great success in computer vision community. CS-MRI reconstruction has been solved by a generalized inverse problem such as image super-resolution (SR) [7] and denoising [1]. A multi-layer Convolutional Neural Network (CNN) has been proposed to recover fully sampled MRI from under-sampled MRI [14]. These existing learning-based CS-MRI methods are driven by a large amount of training samples as a black box without model prior.

Deep unrolling method combines the advantages of model-based and learning-based CS-MRI methods, which has sufficient theoretical support and good performances [16]. ISTA is mapped into deep CNN network to learn proximal mapping [17]. FISTA-Net is designed by mapping FISTA [13] algorithm into a deep network that consists of three update blocks, i.e. gradient descent, proximal mapping and acceleration [15].

However, ISTA-Net+ and FISTA-Net doesn't make full use of other regularization priories (just  $\ell_1$  prior information), and the relationship from optimization theory to network design is also not natural enough. Based on these drawbacks, we start from CS-MRI problem and transform it into a problem that distills features of different geometric characteristic domains and naturally corresponds to the design of our network. The main contributions of this work can be summarized as follows

- (1) We propose a novel deep geometric distillation network, which can not only be theoretically guaranteed to improve partial geometric texture details, but also give us a new perspective to design network structures.
- (2) We compensate the lost texture information from different geometric characteristic domains by designing a geometric distillation module, which is inspired by Taylor expansion of the nonlinear geometric operator.
- (3) All parameters in the proposed method are learnable and these designed constraints can be used to ensure converging smoothly.

## 2 Methodology

The goal of this work is to achieve MRI reconstruction based on Compressive Sensing theory and deep CNN framework. The overall architecture of our deep geometric distillation network is shown in Fig.1, and more details are provided hereafter.

### 2.1 Iterative CS-MRI Reconstruction

General CS-MRI reconstruction can be formulated as the following optimization problem

$$\min_{\mathbf{x}} \{\mathcal{E}(\mathbf{x}) := \mathcal{S}(\mathbf{x}) + \gamma \mathcal{R}(\mathbf{x})\}, \quad (1)$$

where  $\mathbf{x} \in \mathbb{R}^N$  represents a reconstruction of the target MRI,  $\mathcal{S}(\mathbf{x}) = \frac{1}{2} \|\mathcal{F}\mathbf{x} - \mathbf{y}\|_2^2$  is a data fidelity term and  $\mathcal{R}(\mathbf{x})$  is a regularizer with data prior,  $\mathbf{y} \in \mathbb{R}^M (M \ll N)$  represents the under-sampled  $k$ -space data,  $\mathcal{F} \in \mathbb{R}^{M \times N}$  is an under-sampled Fourier measurement matrix,  $\gamma$  is a regularization parameter. Moreover, for iteration stage  $\ell$ ,  $\mathcal{S}_\ell(\mathbf{x})$  is the second-order Taylor expansion of  $\mathcal{S}(\mathbf{x})$  at  $\mathbf{x}_{\ell-1}$ , which is denoted by

$$\mathcal{S}(\mathbf{x}) \approx \mathcal{S}_\ell(\mathbf{x}) = \frac{1}{2\eta_\ell} \|\mathbf{x} - (\mathbf{x}_{\ell-1} - \eta_\ell \mathcal{F}^T (\mathcal{F}\mathbf{x}_{\ell-1} - \mathbf{y}))\|_2^2 + c,$$

hence we can obtain the solution of (1) via two-step iterations

$$\mathbf{m}_\ell = \mathcal{D}(\mathbf{x}_{\ell-1}, \eta_\ell, \mathbf{y}, \mathcal{F}) := \arg \min_{\mathbf{x}} \mathcal{S}_\ell(\mathbf{x}), \quad (2)$$

$$\mathbf{x}_\ell = \mathcal{P}_\lambda(\mathbf{m}_\ell) := \arg \min_{\mathbf{x}} \left\{ \frac{1}{2} \|\mathbf{x} - \mathbf{m}_\ell\|_2^2 + \lambda_\ell \mathcal{R}(\mathbf{x}) \right\} \quad (3)$$

where  $1/\eta_\ell$  is a Lipschitz constant,  $c$  is a constant w.r.t  $\mathbf{x}_{\ell-1}$  and  $\lambda_\ell = \eta_\ell \gamma$ .

### 2.2 Deep Geometric Distillation Network

One alternative to the above iterative optimization scheme is to perform a linear reconstruction module  $\mathcal{D}$  followed by a learned feature compensation module  $\mathcal{P}_\lambda$ . The module  $\mathcal{D}$  often result in heavy artifacts, while the designed CNN module  $\mathcal{P}_\lambda$  is learned to compensate more texture details.

**Linear reconstruction module  $\mathcal{D}$ :** Most methods to reconstruct an image from its measurements  $\mathbf{y}$  rely mainly on linear reconstruction update (2) with a step-length parameter  $\eta_\ell$  and a deterministic operator  $\mathcal{F}$ . In any practical setting,

to increase network flexibility, the step size  $\eta_\ell$  should be positive and decrease with the increasing of iterations smoothly. There are a variety of ways to use training data to adaptively learn parameters  $\eta_\ell$ . Here we employ the **softplus** function  $sp(z) = \ln(1 + \exp(z))$  [15] to make the proposed network converge properly. Mathematically, we rewritten (2) as

$$\mathbf{m}_\ell = \mathcal{D}(\mathbf{x}_{\ell-1}, \eta_\ell, \mathbf{y}, \mathcal{F}) = \mathbf{x}_{\ell-1} - \eta_\ell \mathcal{F}^T (\mathcal{F} \mathbf{x}_{\ell-1} - \mathbf{y}) \quad (4)$$

with a learnable step-length  $\eta_\ell$ , and its initial guess is given as follow

$$\eta_\ell = sp(c_1 \ell + c_2), \quad c_1 < 0, \quad \ell = 1, 2, \dots, \mathcal{N}_\ell. \quad (5)$$

**Geometric distillation module  $\mathcal{P}_\lambda$ :** On the basis of data module  $\mathcal{D}$ , we further propose a prior feature compensation module to compensate for lost texture details. By partially distilling the components from output  $\mathbf{m}_\ell$  of data module  $\mathcal{D}$ , we can obtain feature maps originating from different sparse domains in different stages. Then, these features are aggregated into  $\mathbf{m}_\ell$  to purify and gain more abundant and efficient geometric information.

We recall the optimal condition of (3) as

$$\mathbf{x}_\ell - \mathcal{W}(\mathbf{x}_\ell) = \mathbf{m}_\ell,$$

where  $\mathcal{W}(\mathbf{x}) = -\lambda_\ell \frac{\partial \mathcal{R}(\mathbf{x})}{\partial \mathbf{x}}$  represents the geometric characteristics of  $\mathbf{x}$ . Since  $\mathcal{W}(\mathbf{x})$  is non-linear, it is difficult to directly obtain the close-form solution  $\mathbf{x}_\ell = (I - \mathcal{W})^{-1}(\mathbf{m}_\ell)$  from an input  $\mathbf{m}_\ell$ . Naturally, if the operator  $\mathcal{W}$  satisfies the spectral constraint  $\|\mathcal{W}\| < 1$ , thus we can simplify operator  $(I - \mathcal{W})^{-1}$  by using Taylor expansion as follow:

$$\begin{aligned} \mathbf{x}_\ell &= (I - \mathcal{W})^{-1}(\mathbf{m}_\ell) = \left( \sum_{i=0}^n \mathcal{W}^i + R(\mathcal{W}^n) \right) (\mathbf{m}_\ell) \\ &\in \text{span}(\mathbf{m}_\ell, \mathcal{W}(\mathbf{m}_\ell), \dots, \mathcal{W}^n(\mathbf{m}_\ell), R(\mathcal{W}^n)), \end{aligned} \quad (6)$$

where  $R(\mathcal{W}^n)$  is the remainder of Taylor's expansion and is replaced by  $\mathcal{W}^{n+1}(\mathbf{m}_\ell)$ .

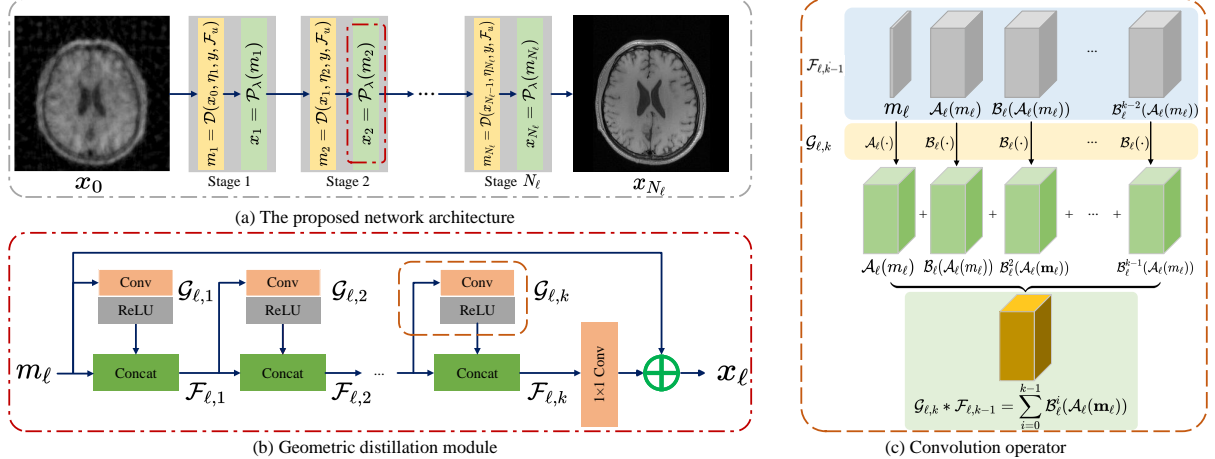


Figure 1: The overall architecture of deep geometric distillation network for Compressive Sensing MRI reconstruction.

The geometric texture information in different sparse (geometric) domains can be represented by the partial derivatives of MRI image  $\mathbf{x}$ . Fortunately, the convolution in neural network can be seen as the combination of several derivative operations. Next we hope to design a network operator  $\mathcal{G}_\ell(\mathbf{m}_\ell)$  (or  $\mathcal{G}_{\ell,k}$ ) replacing  $\mathcal{W}$  for compensating lost geometric characteristics of  $\mathbf{x}_\ell$ . This approach is advantageous because the learning of  $\mathcal{G}_{\ell,k}$  has a large impact on the quality of the reconstruction.

Let  $\text{Concat}(\cdot, \cdot)$  be a concatenate operator as follow

$$\text{Concat}(\mathbf{f}_1, \mathbf{f}_2) = (\mathbf{f}_1, \mathbf{f}_2) \in \mathbb{R}^{n \times m \times s}$$

where  $\mathbf{f}_1 \in \mathbb{R}^{n \times m \times s_1}$ ,  $\mathbf{f}_2 \in \mathbb{R}^{n \times m \times s_2}$  and  $s = s_1 + s_2$ . Let  $\mathcal{F}_{\ell,i}$  be the feature map of the layer  $i$  in stage  $\ell$  defined by

$$\begin{aligned} \mathcal{F}_{\ell,0} &= \mathbf{m}_\ell, \quad \mathcal{F}_{\ell,1} = (\mathbf{m}_\ell, \mathcal{A}_\ell(\mathbf{m}_\ell)), \\ \mathcal{F}_{\ell,i} &= (\mathbf{m}_\ell, \mathcal{A}_\ell(\mathbf{m}_\ell), \dots, \mathcal{B}_\ell^{i-1}(\mathcal{A}_\ell(\mathbf{m}_\ell))), \quad i \geq 2, \end{aligned}$$

where  $\mathcal{A}_\ell$  and  $\mathcal{B}_\ell$  are two blocks with the convolution  $\kappa$  and Rectified Linear Unit (ReLU) such that

$$\begin{aligned}\mathcal{A}_\ell(\cdot) &:= \text{ReLU}(\kappa(\cdot)) : \mathbb{R}^{n \times m} \rightarrow \mathbb{R}^{n \times m \times p}, \\ \mathcal{B}_\ell(\cdot) &:= \text{ReLU}(\kappa(\cdot)) : \mathbb{R}^{n \times m \times p} \rightarrow \mathbb{R}^{n \times m \times p}, \\ \mathcal{B}_\ell^{i-1} &= \underbrace{\mathcal{B}_\ell \circ \dots \circ \mathcal{B}_\ell}_{i-1}, \quad \mathcal{G}_{\ell,i} = \underbrace{(\mathcal{A}_\ell, \mathcal{B}_\ell, \dots, \mathcal{B}_\ell)}_i, \\ \mathcal{F}_{\ell,i} &= \text{Concat}(\mathcal{F}_{\ell,i-1}, \mathcal{G}_{\ell,i} * \mathcal{F}_{\ell,i-1}) \\ &= \text{Concat} \left( \mathcal{F}_{\ell,i-1}, \sum_{j=0}^{i-1} \mathcal{B}_\ell^j(\mathcal{A}_\ell(\mathbf{m}_\ell)) \right),\end{aligned}$$

where the convolution operation  $\mathcal{G}_{\ell,i}$  of the layer  $i$  is employed to recover the lost information of different sparse domains. Finally, an  $1 \times 1$  convolution  $\mathcal{T}_\ell$  defined by  $\mathcal{T}_\ell = (\mathcal{T}_\ell^0, \mathcal{T}_\ell^1, \dots, \mathcal{T}_\ell^k)$  is used to fuse features  $\mathcal{F}_{\ell,k}$ , i.e.

$$\begin{aligned}\mathbf{x}_\ell &= \mathcal{T}_\ell * \mathcal{F}_{\ell,k} = \mathcal{T}_\ell * \text{Concat} \left( \mathcal{F}_{\ell,k-1}, \sum_{j=0}^{k-1} \mathcal{B}_\ell^j(\mathcal{A}_\ell(\mathbf{m}_\ell)) \right) \\ &= \mathcal{C}_\ell^0 * \mathbf{m}_\ell + \sum_{j=1}^k \left( \mathcal{C}_\ell^j * \mathcal{B}_\ell^{j-1}(\mathcal{A}_\ell(\mathbf{m}_\ell)) \right) = \sum_{j=0}^k \mathcal{C}_\ell^j \mathcal{G}_\ell^j(\mathbf{m}_\ell),\end{aligned}$$

where each  $1 \times 1$  convolution  $\mathcal{C}_\ell^i$  in  $\mathcal{C}_\ell = (\mathcal{C}_\ell^0, \mathcal{C}_\ell^1, \dots, \mathcal{C}_\ell^k)$  is a linear combination of  $\{\mathcal{T}_\ell^j\}_{j=0}^k$ . The above operator  $\mathcal{G}_\ell(\mathbf{m}_\ell)$  embedded by many convolution blocks and ReLU layers can be learned as a more flexible representation of the non-linear operation  $\mathcal{W}$  in (6).

**Loss Function.** The loss function is commonly employed to seek the real target image by minimizing the distance measure including pixel-based  $\ell_1$ -norm and  $\ell_2$ -norm between the final reconstructed output  $\mathbf{x}_f$  and the ground truth  $\mathbf{x}$ . However, the capability of pixel-based  $\ell_2$ -norm to capture perceptually relevant components, such as high-frequency geometric details, is insufficient because they are defined on basis of pixel-wise image differences [9].

Here we adopt  $\ell_1$ -loss rather than  $\ell_2$ -loss to enlarge the original loss and add a constraint in the middle of iteration to make the optimization process more compliant. For the given training samples  $\{(\mathbf{y}^i, \mathbf{x}^i)\}_{i=1}^{\mathcal{N}_s}$ , the total loss is defined by

$$\mathcal{L} = \frac{1}{\mathcal{N}_s \mathcal{N}} \sum_{i=1}^{\mathcal{N}_s} \left( \|\mathbf{x}_{\mathcal{N}_\ell}^i - \mathbf{x}^i\|_1 + \|\mathbf{x}_f^i - \mathbf{x}^i\|_1 \right), \quad (7)$$

where  $\mathcal{N}_s$  is the sample number of training set,  $\mathcal{N}$  is the size of  $\mathbf{x}^i$ ,  $\mathcal{N}_\ell = \frac{\mathcal{N}_\ell+1}{2}$  and  $\mathcal{N}_\ell$  is the stage number of our method.

**Parameters and Initialization.** The learnable parameters of the proposed method are denoted as  $\Theta = \{\eta_\ell, \mathcal{A}_\ell, \mathcal{B}_\ell, \mathcal{C}_\ell\}_{\ell=1}^{\mathcal{N}_\ell}$ . The convolution network is initialized with Xavier algorithm. Moreover,  $c_1$  and  $c_2$  are initialized with  $-0.2$  and  $0.1$ , respectively.  $p$ ,  $k$  and  $\mathcal{N}_\ell$  are set to  $32$ ,  $8$  and  $11$ , respectively.

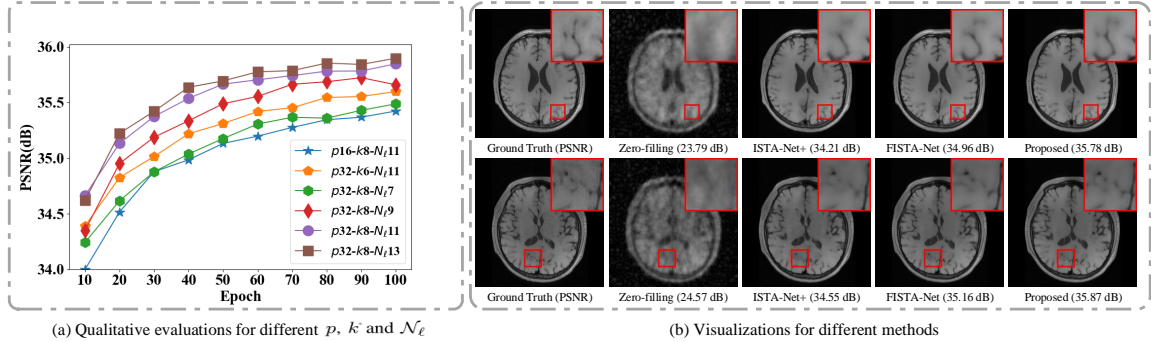


Figure 2: Comparisons of different network parameters and different methods for brain MR images from CS Ratio 10%.

Table 1: Average performance comparisons with different CS ratios for CS-MRI.

Index	Method	CS Ratio				
		10%	20%	30%	40%	50%
PSNR	Zero-filling	26.64 $\pm$ 3.79	30.28 $\pm$ 3.79	32.89 $\pm$ 3.84	35.01 $\pm$ 3.89	36.92 $\pm$ 3.93
	ISTA-Net+	34.83 $\pm$ 4.01	38.75 $\pm$ 3.86	40.99 $\pm$ 3.71	42.64 $\pm$ 3.64	44.22 $\pm$ 3.60
	FISTA-Net	35.15 $\pm$ 3.88	38.84 $\pm$ 3.78	40.99 $\pm$ 3.75	42.61 $\pm$ 3.65	44.03 $\pm$ 3.47
	Proposed	<b>35.85<math>\pm</math>4.12</b>	<b>39.26<math>\pm</math>3.87</b>	<b>41.30<math>\pm</math>3.72</b>	<b>42.81<math>\pm</math>3.64</b>	<b>44.32<math>\pm</math>3.57</b>
SSIM	Zero-filling	0.5733 $\pm$ 0.1335	0.6948 $\pm$ 0.1198	0.7736 $\pm$ 0.1068	0.8268 $\pm$ 0.0933	0.8651 $\pm$ 0.0802
	ISTA-Net+	0.9047 $\pm$ 0.0489	0.9492 $\pm$ 0.0240	0.9639 $\pm$ 0.0167	0.9726 $\pm$ 0.0127	0.9795 $\pm$ 0.0097
	FISTA-Net	0.9115 $\pm$ 0.0459	0.9502 $\pm$ 0.0233	0.9642 $\pm$ 0.0169	0.9726 $\pm$ 0.0128	0.9792 $\pm$ 0.0096
	Proposed	<b>0.9194<math>\pm</math>0.0452</b>	<b>0.9529<math>\pm</math>0.0226</b>	<b>0.9656<math>\pm</math>0.0160</b>	<b>0.9737<math>\pm</math>0.0124</b>	<b>0.9802<math>\pm</math>0.0095</b>

### 3 Experiments and results

We conducted a few experiments to compare the proposed methods with the state-of-the-art methods. Peak signal to noise ratio (PSNR) and Structural Similarity Index Measure (SSIM) are employed to evaluate their performances.

We evaluate the performances of different methods on the widely used brain MR dataset [3] for training within 800 MR brain medical images and testing within 50 images as ISTA-Net+ [17]. They are T1-weighted 2D images from health and Alzheimer’s disease individuals from different MRI devices. We denote the sampling matrix by  $\mathcal{F} = PF$ , where  $P$  is an under-sampling matrix and  $F$  is a discrete Fourier transform.

We use Pytorch to implement our method separately for different CS ratios with batch size 1. We use Adam optimization [10] with a learning rate of 0.0001 to train network for 100 epochs. All experiments are performed on a workstation with Intel Xeon CPU E5-2630 and Nvidia Tesla V100 GPU.

Firstly, we study the reconstruction performances of different basic network parameters ( $p$ ,  $k$  and  $\mathcal{N}_\ell$ ) for brain MR images in CS Ratio 10%. As shown in Fig.2(a), a larger  $p$ ,  $k$  and  $\mathcal{N}_\ell$  achieve quicker convergence and better reconstruction PSNR values. When  $\mathcal{N}_\ell \geq 11$ , the improvement of reconstruction performance becomes slowly with increasing of  $\mathcal{N}_\ell$ . The proposed method allows deeper and wider networks without overfitting, and higher performance can be obtained by extracting more hierarchical features.

We compare the proposed method with Zero-filling [4] and state-of-the-art unrolling methods (ISTA-Net+ [17], FISTA-Net [15]). The CS reconstruction performances corresponding to five CS ratios are shown in Table 1. FISTA-Net performs better than ISTA-Net+ in low CS ratios of 10% and 20%. Our method outperforms FISTA-Net and ISTA-Net+ in all CS ratios obviously.

In Fig.2(b), we show the brain MRI reconstruction results of these methods in CS ratio of 10%, which are consist of total image with a zoom-in details. Zero-filling can remove some noise, but it does not recover the rich texture information very well. Although FISTA-Net and ISTA-Net+ are good at reconstructing MRI from CS measurement, the details are still not good enough. The proposed method can achieve more better reconstruction performance and recover more geometric characteristics.

### 4 Conclusions

In this study, we focus on the classical model-based CS-MRI optimization problem and propose a novel deep geometric distillation CS-MRI reconstruction network. The proposed method combines the merits of model-based CS-MRI method with sampling constraints and deep learning-based CS-MRI method with powerful learning ability. We unfold CS-MRI optimization problem and design deep compensation module to extract lost texture details in the linear reconstruction stage from different geometric characteristic domains. This combination can give us a new perspective to design the explainable network. Experimental validations on the public brain datasets demonstrate the potential of the proposed network both in terms of qualitative and quantitative results.

### Acknowledgment

This work was supported by the National Natural Science Foundation of China (NSFC Project no.11771369, no.12071402 and no.11931003), also partly by grants from the outstanding young scholars of Education Bureau of Hunan Province, P. R. China (number 17B257) and Natural Science Foundation of Hunan Province, P. R. China

(2018JJ2375, 2018XK2304, 2020JJ2027 and 2018WK4006) and Hunan Provincial Innovation Foundation For Post-graduate (number XDCX2021B097).

## References

- [1] F. AGOSTINELLI, M. ANDERSON, AND H. LEE, *Adaptive multi-column deep neural networks with application to robust image denoising*, Advances in Neural Information Processing Systems, (2013).
- [2] A. BECK AND M. TEBOULLE, *A fast iterative shrinkage-thresholding algorithm for linear inverse problems*, SIAM Journal on Imaging Sciences, 2 (2009), pp. 183–202.
- [3] C. BERMUDEZ, S. W. REMEDIOS, K. RAMADASS, M. MCHUGO, S. HECKERS, Y. HUO, AND B. A. LANDMAN, *Generalizing deep whole-brain segmentation for post-contrast mri with transfer learning*, Journal of Medical Imaging, 7 (2020), p. 064004.
- [4] M. A. BERNSTEIN, S. B. FAIN, AND S. J. RIEDERER, *Effect of windowing and zero-filled reconstruction of MRI data on spatial resolution and acquisition strategy*, Journal of Magnetic Resonance Imaging, 14 (2001), pp. 270–280.
- [5] K. T. BLOCK, M. UECKER, AND J. FRAHM, *Undersampled radial MRI with multiple coils. iterative image reconstruction using a total variation constraint*, Magnetic Resonance in Medicine, 57 (2007), pp. 1086–1098.
- [6] S. BOYD, *Distributed optimization and statistical learning via the alternating direction method of multipliers*, Foundations and Trends® in Machine Learning, 3 (2010), pp. 1–122.
- [7] C. DONG, C. C. LOY, K. HE, AND X. TANG, *Image super-resolution using deep convolutional networks*, IEEE Transactions on Pattern Analysis and Machine Intelligence, 38 (2016), pp. 295–307.
- [8] D. DONOHO, *Compressed sensing*, IEEE Transactions on Information Theory, 52 (2006), pp. 1289–1306.
- [9] K. JIANG, Z. WANG, P. YI, J. JIANG, J. XIAO, AND Y. YAO, *Deep distillation recursive network for remote sensing imagery super-resolution*, Remote Sens., 10 (2018), p. 1700.
- [10] D. KINGMA AND J. BA, *Adam: A method for stochastic optimization*, International Conference on Learning Representations, (2014).
- [11] Z. LAI, X. QU, Y. LIU, D. GUO, J. YE, Z. ZHAN, AND Z. CHEN, *Image reconstruction of compressed sensing MRI using graph-based redundant wavelet transform*, Medical Image Analysis, 27 (2016), pp. 93–104.
- [12] S. G. LINGALA AND M. JACOB, *Blind compressive sensing dynamic MRI*, IEEE Transactions on Medical Imaging, 32 (2013), pp. 1132–1145.
- [13] M. LUSTIG, D. DONOHO, AND J. M. PAULY, *Sparse MRI: The application of compressed sensing for rapid MR imaging*, Magnetic Resonance in Medicine, 58 (2007), pp. 1182–1195.
- [14] S. WANG, Z. SU, L. YING, X. PENG, S. ZHU, F. LIANG, D. FENG, AND D. LIANG, *Accelerating magnetic resonance imaging via deep learning*, 2016 IEEE 13th International Symposium on Biomedical Imaging (ISBI), (2016).
- [15] J. XIANG, Y. DONG, AND Y. YANG, *FISTA-net: Learning a fast iterative shrinkage thresholding network for inverse problems in imaging*, IEEE Transactions on Medical Imaging, (2021), pp. 1–1.
- [16] Y. YANG, J. SUN, H. LI, AND Z. XU, *Deep admm-net for compressive sensing mri*, Advances in Neural Information Processing Systems, (2016).
- [17] J. ZHANG AND B. GHANEM, *ISTA-net: Interpretable optimization-inspired deep network for image compressive sensing*, 2018 IEEE/CVF Conference on Computer Vision and Pattern Recognition, (2018).